Supplemental Data 1. Solution molecular mass of Lhx3/4-Isl1/2 complexes

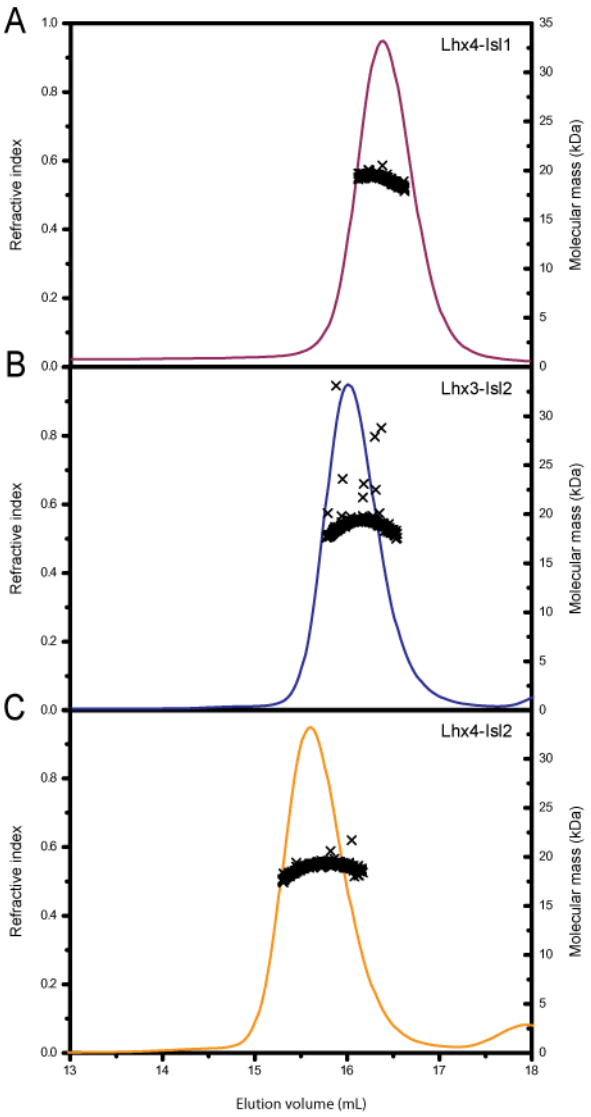

Figure S1 Molecular mass analysis of Lhx3/4-Isl1/2 complexes. The constructs (**A**) Lhx4-Isl1, (**B**) Lhx3-Isl2 and (**C**) Lhx4-Isl2 were subjected to size-exclusion chromatography with in-line multi-angle laser light scattering. Protein concentration was measured in refractive index units (continuous line) and the calculated weight-average molecular mass was determined from the amount of light scattered (×). Data for Lhx3-Isl1 were reported in (1).

Supplemental Data 2. Residues missing electron density in PDB submission 3MMK

Table S2A List of residues missing entirely from structure

Lhx4 (24–149)		**Isl2** (272–301)		**Tag[a]/Linker[b]**	
Chain A	**Chain B**	**Chain A**	**Chain B**	**Chain A**	**Chain B**
Met24	Met24	Pro300		Gly22	Gly22
Gln25	Gln25	Trp301		Ser23	Ser23
Pro97				Gly261	Gly261
Pro98				Gly262	Gly262
Gln149	Gln149			Ser263	Ser263
				Gly264	Gly264
				Gly265	Gly265
				Met266	Met266
				His267	His267
				Gly268	Gly268
				Ser269	Ser269
					Gly270

[a]Residues 22 and 23 are left at the N-terminus of the protein after cleavage of the GST tag using thrombin.
[b]Residues 261–271 are a part of the Gly/Ser-linker used to tether $Lhx4_{LIM1+2}$ with $Isl2_{LBD}$. Gly261 follows Gln149 of Lhx4.

Table S2B List of residues missing atoms from sidechains

Lhx4		**Isl2**	
Chain A	**Chain B**	**Chain A**	**Chain B**
Gln26	Gln26	Glu284	Glu284
Leu46	Leu46		Asn285
Asp47	Asp47	Gln288	
Lys56	Lys56	Glu293	
	Asp59	Tyr297	
Gln61	Gln61	Gln298	
Met62	Met62	Pro299	
Gln63	Gln63		
Ala65			
Arg71	Arg71		
Lys78	Lys78		
Glu79	Glu79		
Phe82			
Lys83	Lys83		
Arg84	Arg84		
	Phe85		
Lys88	Lys88		
Thr99			
Gln100			
Lys104			
	Asp107		
Arg122	Arg122		
Glu134	Glu134		
Lys148	Lys148		

Supplemental Data 3. The solution structure of Lhx3/4-Isl1/2 tethered complexes

Proteins were subjected to size-exclusion chromatography prior to SAXS analysis, using a Superdex 75 (10/300) size-exclusion column (GE Healthcare) in a running buffer of 20 mM Tris.HCl (pH 8.5), 150 mM NaCl and 0.5 mM TCEP. The samples used for collecting the scattering data were analysed immediately after elution from the column and the protein sample was taken from the second half of the peak to favour collection of a monodisperse solution. A protein-free fraction from the size-exclusion column was used as a solvent blank for the SAXS experiments. As the Lhx4-Isl2 solution used for the collection of scattering intensities was found to be monodisperse (Table II and Figure S3A), shape information could be deduced from the scattering data of the protein in solution.

A reasonable solution for the $P(r)$ transformation of the Lhx4-Isl2 scattering data was obtained using the program GIFT with a maximum dimension (D_{max}) of 77 Å, yielding a R_g of 23.5 Å (Figure 5A and Table S3). These SAXS-derived structural parameters are significantly larger than those calculated from the 'bent' conformation observed in the crystal structure (R_g = 20.5 Å, D_{max} = 70–75; Figure 5A and Table S3). Thus, on average in solution Lhx4-Isl2 adopts a more extended conformation than in the crystal structure. The $P(r)$ transform does not exhibit the shoulder that would be evident if there were relatively fixed inter-atomic distances between two domains as calculated for the crystal structure (r ~35 Å). The absence of the shoulder likely results from variability in the inter-domain distances due to flexibility at the hinge/spacer. Overall the SAXS data indicate that the overall shape and relative orientations of the two halves of the complex (LIM1 and LIM2 with their corresponding binding motifs in $Isl2_{LBD}$) in the crystal structure do not represent the average conformation of the molecule in solution.

Rigid-body refinement of the position of the two halves of Lhx4-Isl2 with respect to each other against the SAXS data was performed using BUNCH. The program used a simulated annealing protocol in which the two halves of the complex were allowed to assume different relative orientations around the hinge/spacer between the two domains. This process was performed in two rounds. In the first round the program modelled dummy atoms in the GS-rich linker and at the N-terminal end of the protein that were missing from the crystal structure by refining the average position of the mass of the missing regions against the scattering intensities. In the second round the structure was split in half through the hinge/spacer to

produce LIM1-peptide and LIM2-peptide modules, where the peptide was the corresponding binding sequence from $Isl2_{LBD}$. Residues 287–290 of $Isl2_{LBD}$ were excised and modelled as dummy atoms to provide greater freedom in generating flexion between the two LIM-peptide modules during refinement. To ensure that BUNCH only modelled conformations that are physically possible for the molecule to adopt, the following distance restraints were specified to restrict the distances that elements of the molecule could be moved apart: $Isl2_{A276}$ and $Isl2_{A291}$ = 16.5 Å; $Lhx4_{G86}$ and $Lhx4_{T87}$ = 4.5 Å; $Isl2_{E274}$ and $Lhx4_{F82}$ = 16.5 Å. These distance restraints effectively provide the connectivity that would otherwise be contributed by the missing residues in the hinge/spacer, and were evident in the resulting BUNCH-generated interface of the two LIM/peptide modules.

Refinements were run multiple times and each independent calculation converged toward a consensus extended conformation with a significantly improved fit to the data that does not show the deviations in the very-low- and mid-*q* regimes observed for the crystal structure fit (Figure S3B). The χ^2-value is significantly improved (0.52 compared to 0.70 obtained for the comparison with the crystal structure) and the structural parameters of the BUNCH model are much more similar than those of the crystal structure to the scattering data (Figure 5A and B and Table S3).

Similar SAXS data were measured for Lhx3-Isl2 and Lhx3-Isl1, which also suggested there is flexibility in the structures (Figure 5C and Figure S3A). Data were not analysed for Lhx4-Isl1 because the protein aggregated at the concentrations required for SAXS analysis (>0.8 mg mL^{-1}). As there is no present crystal structure for Lhx3-Isl2, the BUNCH refinement was performed using the Lhx3-Isl1 structure. For the BUNCH refinements of both Lhx3-Isl1 and Lhx3-Isl2, residues 83–92 of $Lhx3_{LIM1+2}$ were excised and modelled as dummy atoms. The following distance restraints were specified during refinement: $Isl1_{R272}$ and $Isl2_{H273}$ = 12.0 Å; $Lhx3_{F82}$ and $Lhx3_{T87}$ = 11.5 Å; $Lhx3_{F82}$ and $Lhx3_{P97}$ = 12.0 Å.

Again the resultant BUNCH models provide significantly improved fits to the data than the crystal structure, particularly in the very-low- and mid-*q* regions (Figure S3B). The χ^2-value of the Lhx3-Isl1 BUNCH model profile with respect to the scattering data is 0.60 compared to 1.55 for the crystal structure. The BUNCH models for Lhx3-Isl1 and Lhx3-Isl2 show a significantly improved correspondence with the experimentally derived structural parameters (Figure 5C–E and Table S3). Interestingly, the Lhx3-Isl2

BUNCH model shows the same degree of compactness as the Lhx4-Isl2 BUNCH model relative to that of Lhx3-Isl1, despite using the structural information from Lhx3-Isl1 in the modelling.

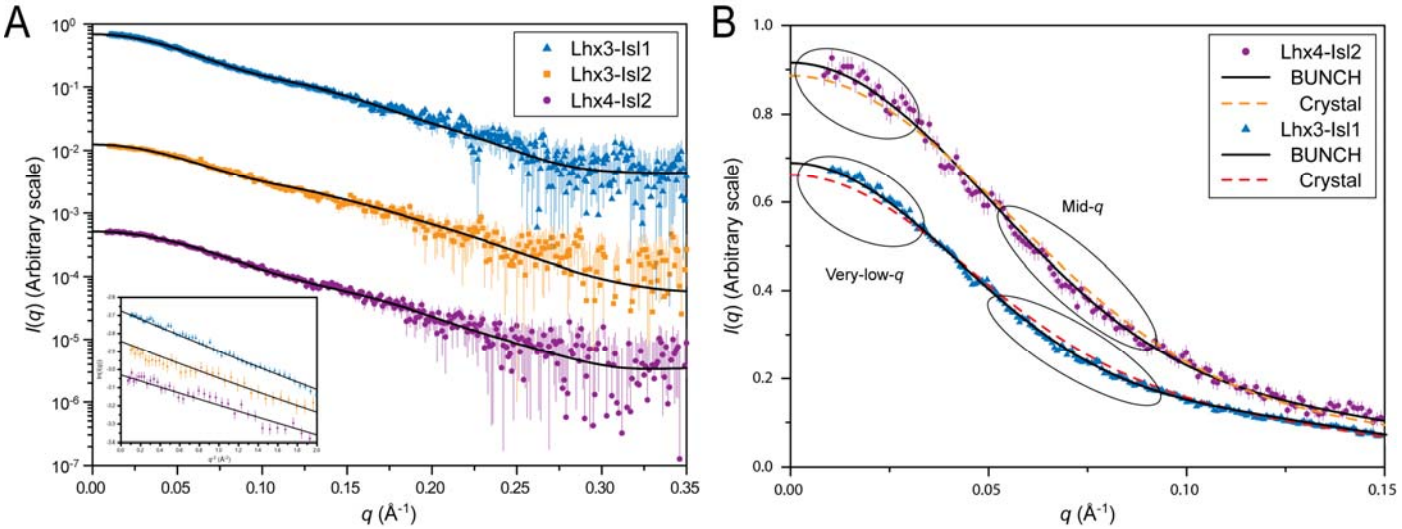

Figure S3 (**A**) Scattering data for Lhx3-Isl1 (light blue), Lhx3-Isl2 (orange) and Lhx4-Isl2 (purple) shown as $I(q)$ against q with Guinier plots ($\ln(I(q))$ against q^2) in the inset. The black curves are the best-fit BUNCH models for each dataset. (**B**) Scattering data from A replotted to illustrate the deviation of the crystal structure fits to the experimental scattering data (orange dashed line for Lhx4-Isl2, red dashed line for Lhx3-Isl1) and the improved fit of the BUNCH model data in the very-low- and mid-q regimes. In all plots the curves have been shifted on the vertical axis for clarity

Table S3 Structural parameters of the Lhx-Isl$_{LBD}$ proteins and the models used

	Lhx3-Isl1			*Lhx3-Isl2*			*Lhx4-Isl2*		
	R_g (Å)	D_{max} (Å)	χ^2	R_g (Å)	D_{max} (Å)	χ^2	R_g (Å)	D_{max} (Å)	χ^2
Crystal	23.6	84	1.55	N/A	N/A	N/A	20.5	72	0.70
BUNCH	26.2	90	0.60	23.4	78	0.54	22.6	76	0.52
Scattering	26.9	89	N/A	22.3	75	N/A	23.5	77	N/A

Supplemental Data 4. Mutational screening of Lhx3/4:Isl1/2 interactions using yeast two-hybrid analysis. $Isl1_{LBD}$ and $Isl2_{LBD}$ and a suite of mutants were screened for their ability to bind the LIM domains of Lhx3 and Lhx4 as indicated (Table S4). Results for the individual LIM domains of Lhx3 and Lhx4 are reported in the main text. For the mutants, sets of three sequential residues were mutated to alanine (or glycine if the wild-type residue was alanine). These mutants were designated m1a through to m1j for Isl1 and m2a through to m2j for Isl2 (Table S4). For those triple mutants where significantly reduced binding was observed (m1b, m2b and m2h) single point mutants were tested to pin-point the residues responsible for the reduction of binding.

Isl1 versus Lhx3. The binding of Isl1 mutants to Lhx3 has been reported previously (1) and the data are presented here for comparison. Only m1b of the triple mutants significantly reduced binding, and the key binding residues were identified as $Isl1_{M265}$ and $Isl1_{A267}$.

Isl1 versus Lhx4. The data for the binding of Isl1 mutants to Lhx4 is reported here. Of the triple mutants, again only m1b showed significant reduction in binding. Of the single mutants, $Isl1_{A267G}$ significantly disrupted the interaction with Lhx4 compared to the wild-type, and both $Isl1_{M265A}$ and $Isl1_{V266A}$ had a weak effect on binding (Table S4). Four $Isl1_{LBD}$ triple-mutant constructs (m1c, m1f, m1g, and m1j) that reduced binding to Lhx3 under high stringency conditions did not appear to significantly disrupt the interaction with $Lhx4_{LIM1+2}$ (Table S4).

Isl2 versus Lhx3 and Lhx4. Of the triple mutants, m2b and m2h showed significantly reduced binding to both Lhx3 and Lhx4. Of the single mutants, $Isl2_{L275A}$, $Isl2_{V276A}$ and $Isl2_{A277G,}$ all of which lie in the N-terminal half of $Isl2_{LBD}$, showed significantly reduced binding to $Lhx3_{LIM1+2}$ (Table S4). Of these mutants $Isl2_{A277G}$ strongly reduced binding to $Lhx4_{LIM1+2,}$ whereas $Isl2_{L275A}$ and $Isl2_{V276A}$ had a more moderate effect on binding. Individual mutation of Glu293, Val294 or Gln295 in the C-terminal half of $Isl2_{LBD}$ had a weak influence on binding to $Lhx3_{LIM1+2}$ and $Lhx4_{LIM1+2}$, but in combination nearly abolished binding (Table S4). Overall these results suggest that the key binding determinants for $Isl2_{LBD}$ are more evenly distributed over both halves of the interface compared with $Isl1_{LBD}$. Only one of the $Isl2_{LBD}$ triple-mutant constructs (m2d) was found not to disrupt binding to $Lhx3_{LIM1+2}$ or $Lhx4_{LIM1+2}$ under high stringency conditions (Table S4).

$Isl1_{M265L}$ and $Isl2_{L275M}$ mutants. Constructs developed to investigate the preference for methionine or leucine at $Isl1_{M265}$/$Isl2_{L275}$ were generated on a wild-type background (giving $Isl1_{M265L}$ and $Isl2_{L275M}$), or on the background of the m1h and m2h mutants to attempt to make the assay more sensitive to the effect of the Met/Leu mutants. These data indicate a subtle difference in the sequence preferences of Lhx3 and Lhx4. For Lhx3 there was no distinguishable effect of the M→L and L→M mutations in any context, suggesting that Lhx3 has no apparent preference for leucine or methionine at $Isl1_{265}$/$Isl2_{275}$ (Figures 6B and S4 and Table S4). For Lhx4, the $Isl1_{M265L}$ mutation slightly reduced the apparent affinity of Isl1 for Lhx4 on the wild-type background, whereas the $Isl2_{L275M}$ mutation slightly increased the apparent affinity of Isl2 for Lhx4 on both the wild-type and mutant background (Figure 6B, lanes 5 and 6 under high stringency conditions, and Table S4). Further, $Isl2_{L275M}$ showed an interaction with $Lhx4_{LIM2}$ under moderate stringency conditions, whereas wild-type $Isl2_{LBD}$ shows virtually none under low stringency conditions (Figure S4, lanes 7 and 8 under low and moderate stringency conditions). These data suggest that Lhx4 has a minor preference for methionine at $Isl1_{265}$/$Isl2_{275}$.

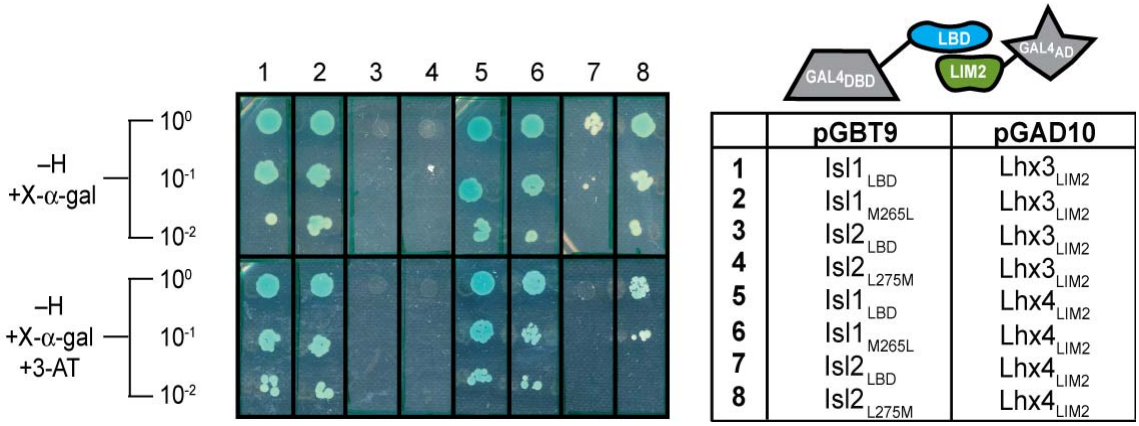

	pGBT9	pGAD10
1	$Isl1_{LBD}$	$Lhx3_{LIM2}$
2	$Isl1_{M265L}$	$Lhx3_{LIM2}$
3	$Isl2_{LBD}$	$Lhx3_{LIM2}$
4	$Isl2_{L275M}$	$Lhx3_{LIM2}$
5	$Isl1_{LBD}$	$Lhx4_{LIM2}$
6	$Isl1_{M265L}$	$Lhx4_{LIM2}$
7	$Isl2_{LBD}$	$Lhx4_{LIM2}$
8	$Isl2_{L275M}$	$Lhx4_{LIM2}$

Figure S4 Yeast two-hybrid assays of the LBDs of Isl1 and Isl2 and $Isl1_{M265L}$ and $Isl2_{L275M}$ mutants LIM2 of Lhx3 and Lhx4 which is not reported in Table S4 below.

Table S4 Detecting the regions and residues mediating interactions between $Isl1_{LBD}$/$Isl2_{LBD}$ and $Lhx3_{LIM1+2}$/$Lhx4_{LIM1+2}$ (see legend on following page).

Binding peptide	Lhx3		Lhx4	
Individual LIM domains	$Lhx3_{LIM1}$	$Lhx3_{LIM2}$	$Lhx4_{LIM1}$	$Lhx4_{LIM2}$
$Isl1_{LBD}$	−/−/−	+++/~/−	−/−/−	+++/+/−
$Isl2_{LBD}$	−/−/−	−/−/−	−/−/−	~/−/−
$Ldb1_{LID}$	+/−/−	+++/+/−	+/−/−	+++/+/−
	$Lhx3_{LIM1+2}$		$Lhx4_{LIM1+2}$	
$Isl1_{LBD}$ (262–291)	DBD	AD	DBD	AD
WT-GTPMVAASPERHDGGLQANPVEVQSYQPPW	+++/−	+++/+++	+++/+	+++/+++/++
Triple mutants				
m1a-AAAMVAASPERHDGGLQANPVEVQSYQPPW	+++/−	+++/−	+++/−	+++/+++/−
m1b-GTPAAGASPERHDGGLQANPVEVQSYQPPW	−/−	−/−	−/−	−/−/−
m1c-GTPMVAGAAERHDGGLQANPVEVQSYQPPW	+++/−	+++/−	+++/−	+++/+++/+
m1d-GTPMVAASPAAADGGLQANPVEVQSYQPPW	+++/−	+++/−	+++/−	+++/+++/−
m1e-GTPMVAASPERHAAALQANPVEVQSYQPPW	+++/−	+++/−	+++/−	+++/+++/−
m1f-GTPMVAASPERHDGGAAGNPVEVQSYQPPW	+++/−	+++/−	+++/++	+++/+++/++
m1g-GTPMVAASPERHDGGLQAAAAEVQSYQPPW	+++/−	+++/−	+++/+	+++/+++/~
m1h-GTPMVAASPERHDGGLQANPVAAASYQPPW	+++/−	+++/−	+/−	+++/+++/−
m1i-GTPMVAASPERHDGGLQANPVEVQAAAPPW	+++/−	+++/−	+++/−	+++/+++/++
m1j-GTPMVAASPERHDGGLQANPVEVQSYQAAA	+++/−	+++/−	+++/−	+++/+++/−
Single point mutants				
M265A-GTP**A**VAASPERHDGGLQANPVEVQSYQPPW	~/−	−/−	++/−	+++/+++/−
V266A-GTPM**A**AASPERHDGGLQANPVEVQSYQPPW	+++/−	+++/−	++/−	+++/+++/−
A267G-GTPMV**G**ASPERHDGGLQANPVEVQSYQPPW	~/−	−/−	~/−	+++/+++/−
M265L mutants				
GTP**L**VAASPERHDGGLQANPVEVQSYQPPW	ND	+++/+++/+++	ND	+++/+++/~
GTP**L**VAASPERHDGGLQANPV**AAA**SYQPPW	ND	+++/+++/−	ND	+++/+++/−
$Isl2_{LBD}$ (272–301)				
WT-GTPLVAGSPIGHENAVQGSAVEVQTYQPPW	+++/+++/−	+++/+++/+	+++/−	+++/+++/+
Triple mutants				
m2a-AAALVAGSPIGHENAVQGSAVEVQTYQPPW	+++/++/−	+++/+++/−	+++/−	+++/+++/−
m2b-GTPAAGGSPIGHENAVQGSAVEVQTYQPPW	−/−/−	−/−/−	−/−	−/−/−
m2c-GTPLVAAAAIGHENAVQGSAVEVQTYQPPW	+++/+++/−	+++/+++/−	+++/−	+++/+++/−
m2d-GTPLVAGSPAAAENAVQGSAVEVQTYQPPW	+++/+++/−	+++/+++/++	+++/−	+++/+++/+
m2e-GTPLVAGSPIGHAAGVQGSAVEVQTYQPPW	+++/+++/−	+++/+++/−	+++/−	+++/+++/−
m2f-GTPLVAGSPIGHENAAAASAVEVQTYQPPW	+++/+/−	+++/+++/−	+++/−	+++/+++/−
m2g-GTPLVAGSPIGHENAVQGAGAEVQTYQPPW	+++/−/−	+++/+/−	+++/−	+++/+++/−
m2h-GTPLVAGSPIGHENAVQGSAVAAATYQPPW	−/−/−	~/−/−	−/−	+++/+/−
m2i-GTPLVAGSPIGHENAVQGSAVEVQAAAPPW	+++/+++/−	+++/+++/−	+++/−	+++/+++/−
m2j-GTPLVAGSPIGHENAVQGSAVEVQTYQAAA	+++/+++/−	+++/+++/−	+++/−	+++/+++/−
Single point mutants				
L275A-GTP**A**VAGSPIGHENAVQGSAVEVQTYQPPW	−/−/−	−/−/−	−/−	+++/++/−
V276A-GTPL**A**AGSPIGHENAVQGSAVEVQTYQPPW	−/−/−	~/−/−	−/−	+++/++/−
A277G-GTPLV**G**GSPIGHENAVQGSAVEVQTYQPPW	−/−/−	−/−/−	−/−	~/−/−
E293A-GTPLVAGSPIGHENAVQGSAV**A**VQTYQPPW	+++/++/−	+++/++/−	+++/−	+++/+++/−
V294A-GTPLVAGSPIGHENAVQGSAVE**A**QTYQPPW	+++/+/−	+++/+/−	++/−	+++/++/−
Q295A-GTPLVAGSPIGHENAVQGSAVEV**A**TYQPPW	+++/+++/−	+++/+++/−	+++/−	+++/+++/~
L275M mutants				
GTP**M**VAGSPIGHENAVQGSAVEVQTYQPPW	ND	+++/+++/+	ND	+++/+++/++
GTP**M**VAGSPIGHENAVQGSAV**AAA**TYQPPW	ND	~/−/−	ND	+++/+++/−

Table S4 legend: Summary of alanine scanning mutagenesis screens of $Isl1_{LBD}$ and $Isl2_{LBD}$ against $Lhx3_{LIM1+2}$ and $Lhx4_{LIM1+2}$ and individual LIM domains of Lhx3 and Lhx4 against $Isl1_{LBD}$, $Isl2_{LBD}$ and

$Ldb1_{LID}$ using the yeast two-hybrid assay. Triple alanine mutants have been designated m1a through to m1j for $Isl1_{LBD}$ and m2a through m2j for $Isl2_{LBD}$. Mutated residues are underlined in the sequences. The stringency of selection conditions was weak (−L−W−H)/moderate (−L−W−H 1 mM 3-AT)/high (−L−W−H−A), except for the previously reported alanine scanning mutagenesis of $Lhx3_{LIM1+2}$/$Isl1_{LBD}$ interactions and those interactions where $Lhx4_{LIM1+2}$ was in pGBT9 in which the stringency was moderate/high. +++ indicates growth in 10^0, 10^{-1} and 10^{-2} dilutions, ++ indicates growth only in 10^0 and 10^{-1}, + indicates growth only in 10^0, ~ indicates minor levels of growth only in 10^0 and − indicates no growth at any dilution used. Individual LIM domains were tested only in pGAD10. Boxed interactions were reported previously (1). In contrast to the results reported in ref (1), when $Lhx3_{LIM2}$ was fused to the Gal4 activation domain (AD; in pGAD10) the interactions observed appeared to be weaker. However, the relative strength of the interactions remains consistent between $Isl1_{LBD}$ and $Ldb1_{LID}$.

References for Supplemental Data

1. Bhati, M., Lee, C., Nancarrow, A. L., Lee, M., Craig, V. J., Bach, I., Guss, J. M., Mackay, J. P., and Matthews, J. M. (2008) *EMBO J* **27**, 2018-2029